GEOPHYSICS, VOL. 72, NO. 1 (JANUARY-FEBRUARY 2007); P. P1–P8, 8 FIGS.
10.1190/1.2387138

Lineament-preserving filtering

Saleh Al-Dossary[1] and Kurt J. Marfurt[1]

ABSTRACT

Recently developed seismic attributes such as volumetric curvature and amplitude gradients enhance our ability to detect lineaments. However, because these attributes are based on derivatives of either dip and azimuth or the seismic data themselves, they can also enhance high-frequency noise. Recently published structure-oriented filtering algorithms show that noise in seismic data can be removed along reflectors while preserving major structural and stratigraphic discontinuities. In one implementation, the smoothing process tries to select the most homogenous window from a suite of candidate windows containing the analysis point. A second implementation damps the smoothing operation if a discontinuity is detected. Unfortunately, neither of these algorithms preserves thin or small lineaments that are only one voxel in width. To overcome this defect, we evaluate a suite of nonlinear feature-preserving filters developed in the image-processing and synthetic aperture radar (SAR) world and apply them to both synthetic and real 3D dip-and-azimuth volumes of fractured geology from the Forth Worth Basin, USA. We find that the multistage, median-based, modified trimmed-mean algorithm preserves narrow geologically significant features of interest, while suppressing random noise and acquisition footprint.

INTRODUCTION

Lineaments are found in nearly every reservoir, rock type, and depth. Petroleum explorationists relate these lineaments to fractures in order to understand their reservoirs. Fractures can advance or hinder our efforts in producing a reservoir, and can be found in source rocks, reservoir rocks, and cap rocks. Locating these fractures and identifying their orientations can help explorationists enhance production of hydrocarbons or avoid production of water. Geometric attributes are particularly effective in delineating lineaments that may be related to fracture zones or subseismic faults (Al-Dossary and Marfurt, 2006; Blumentritt et al., 2006; Sullivan et al., 2006). On seismic time slices, lineaments are often seen as small and thin linear features. Possible causes for the seismic contrast that causes fractures to be visible include gas charge, porosity preservation, stress release, diagenetic alteration, and crack fill.

Seismic attributes such as coherence (e.g., Bahorich and Farmer, 1995), reflector dip (Dalley et al., 1989), amplitude gradients (Luo et al., 1996), and curvature (Al-Dossary and Marfurt, 2006) can all provide images of narrow fractures and other lineaments. Skirius et al. (1999) uses seismic coherence in carbonates in North America and the Arabian Gulf, Luo et al. (2003) uses amplitude gradients on carbonates from Saudi Arabia to delineate faults and other lineaments. Although coherence can often detect lineaments, reflector curvature is more directly linked to fracture distribution (Lisle, 1994; Roberts, 2001; Bergbauer et al., 2003).

Al-Dossary and Marfurt (2006) implemented multiscale volume-based curvature computations and found the most positive and negative curvatures, k_{pos} and k_{neg}, to be the most useful for delineating faults, lineaments, flexures, and folds. Blumentritt et al. (2006) used volumetric curvature attributes to determine the stress regime and the most likely direction of open fractures in a case study applied to west Texas carbonates.

All of these attributes can be contaminated by seismic noise. Noise filtering can generally enhance the behavior of coherence, amplitude gradients, curvature, and other edge-detection algorithms applied to seismic data. The quality of such edge detectors and the reliability of the interpretation are directly related to the effectiveness of the noise reduction filters applied prior to the calculation. The purpose of this paper is to improve the appearance of the short-wavelength estimates of reflector curvature by improving the signal-to-noise ratio while maintaining the narrow, short-wavelength geologic features of interest.

Historically, linear mean and nonlinear median filters have been widely used to improve the interpretability of the seismic data. Unfortunately, the mean filter can severely blur coherence and other edge sensitive attributes. The edge-preserving and impulse-removing properties are the most desirable features of the median filter

Manuscript received by the Editor March 13, 2005; revised manuscript received May 20, 2006; published online November 27, 2006.
[1]University of Houston, Allied Geophysical Laboratories, Room 510, Science and Research Building 1, Cullen Road Entrance 14, Houston, Texas 77204. E-mail: saleh_amr@yahoo.com; kmarfurt@uh.edu.

(Schulze and Pearce, 1991). Although median and related alpha-trim mean filters can preserve edges by separating fault blocks and stratigraphic features that are several traces in width, they will, in general, obliterate narrow curvilinear features associated with joints and fractures that are only a single trace wide.

In SAR applications, simple mean and median filters have been supplanted by more advanced Lee and Frost filters (Frost et al., 1982; Lee, 1986). The more recently published speckle-reducing anisotropic-diffusion filters (Yu and Acton, 2002) also are effective in reducing speckle noise. Although these filters were developed to smooth images with speckle noise, some of them have been modified to smooth images with additive noise. Others have been developed to take care of both kinds of noise.

Luo et al. (2002) generated an edge-preserving smoothing (EPS) algorithm based on Kuwahara et al.'s (1976) multiwindow analysis technique. A good review of the Kuwahara and several of the other filters discussed in this paper can be found in Astola and Kuosmanen (1997). EPS attempts to resolve the conflict between noise reduction and edge degradation via a simple modification of the running-average smoothing method. In principle, EPS looks for the most homogeneous window around each sample in an input data set and assigns the average value of the selected window to that sample (Luo et al., 2002). EPS has been successfully applied to different data sets from Saudi Arabia and other parts of the world. However, Luo et al. (2002) noted that EPS is inadequate in preserving small features that are less than three voxels wide, and stated that genuine geologic features (e.g., channels) would be suppressed if their width were smaller than the window size. If such small features are the desired output after running edge-detection, they recommend using an EPS window that is smaller than the characteristic width of the expected features, or if the features of interest are too small, simply dropping EPS from the processing sequence. Marfurt (2006) generalizes Luo et al.'s (2002) EPS algorithm to include a multiwindow dip search, followed by a principal component filter in the most coherent window. Principal component filtering does an excellent job in preserving one-trace wide lineaments in amplitude, but cannot be generalized readily to enhance lineaments in dip, azimuth, or curvature attributes.

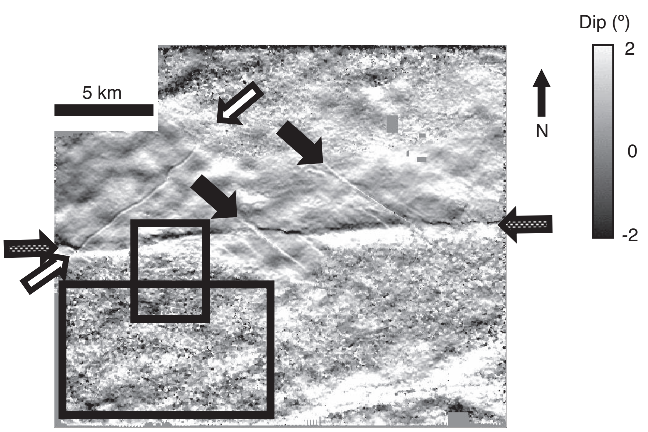

Figure 1. A time slice at $t = 0.8$ s through a north-south dip volume from a survey in the Fort Worth Basin. Dotted arrows indicate a broad east-west strike-slip fault. Solid black arrows indicate thinner northwest-southeast lineaments. White arrows indicate a northeast-southwest channel. Solid rectangles indicate two older, smaller surveys, incorporated into a larger, merged survey. All three surveys were reprocessed as a unit, so data quality differences result from acquisition, rather than processing. (Data courtesy of Devon Energy)

Hoecker and Fehmers (2002) introduced a fourth means of random noise suppression based on the gradient structure tensor (GST) discussed by Bakker et al. (1999). They begin by estimating the reflector dip and azimuth from the GST eigenvectors. If the coherence (or other measure of similarity) is high, they apply a mean filter to the data along the reflector dip and azimuth. If the reflector coherence is low, they apply proportionately less smoothing, with no smoothing applied for large discontinuities. The smoothing and coherence calculation is applied recursively along the reflector dip and azimuth, thereby simulating an annealing process that can be represented by an anisotropic diffusion equation. We have found the anisotropic diffusion algorithm to be quite robust in suppressing random noise while preserving faults, but it exhibits the same limitations as the first three methods when applied to lineaments only one trace in width.

Our work differs from the previous literature in two ways. First, our major focus will be on preserving small lineaments rather than large discontinuities. Second, we will apply lineament-preserving smoothing initially to volumetric components of the reflector dip vector, rather than to the amplitude. Improvements in our vector dip estimate will not only improve our estimates of reflector curvature (Al-Dossary and Marfurt, 2006) but also subsequent computation of principal component filtering, coherent amplitude gradients, and coherence (Marfurt, 2006). With this objective in mind, we have evaluated a wide range of current techniques used in the image processing and synthetic aperture radar (SAR) world and adapted those filters that can reduce noise, preserve edges, and preserve thin lineaments often seen on seismic data.

We begin the next section with a summary of alternative filtering techniques that have been used to smooth seismic data before applying edge detection or coherence computations. Next, we describe some of the more relevant image processing and SAR algorithms. Finally, we apply the three most effective algorithms — the anisotropic diffusion, lower-upper-middle median (LUM), and the multistage median modified-trimmed-mean (MSMTM) filters — to both a synthetic example and a real survey over a fractured karst terrain from the Fort Worth Basin, U.S.A.

REVIEW OF SMOOTHING FILTERS

The mean filter

The mean filter is the simplest and most familiar random-noise-suppression filter. The mean filter is a low-pass filter, which is typically implemented as a running window that outputs the average of all the samples that fall within an analysis window at its center. The window size is usually an odd number, such as 3×3 or 5×5, and may be either rectangular or elliptical. The definition of the mean filter is

$$d_{\text{mean}} = \frac{1}{J}\sum_{j=1}^{J} d_j, \tag{1}$$

where d denotes the jth of J traces falling within the analysis window at time t.

In Figure 1, we show a time slice at 0.8 s through the north-south component of the vector-dip volume calculated using the technique described by Marfurt (2006) over a survey from the Fort Worth Basin, Texas. We note an east-west strike slip fault and a suite of antithetic northwest-southeast narrow lineaments, as well as a northeast-southwest trending channel that was probably also controlled by a fault or fracture. Two small, previously acquired surveys were merged into a newer survey with a more robust acquisition program. We applied four passes of a running (3×3) window mean filter in an attempt to improve the signal-to-noise ratio (Figure 2). Although significantly improving the geologically interesting long-wavelength characteristics of the data, the short-wavelength fracture patterns are smeared, making them difficult to see. In an earlier paper (Al-Dossary and Marfurt; 2006), we discuss the value of multispectral estimates of reflector curvature and find these long-wavelength estimates to be especially revealing of the underlying geology in the Fort Worth Basin. Our goal in this paper is to improve the appearance of the short-wavelength estimates of reflector curvature through nonlinear noise suppression.

To better illustrate our evaluation of alternative-filtering schemes, we extract a small part of the northwest corner of Figure 1 and redisplay it as Figure 3a. Then we generate an idealized synthetic in Figure 3b, where we represent the east-west strike-slip fault as three traces wide, the narrow northwest-southeast lineaments as either one or two traces wide, and a meandering northeast-southwest channel as one trace wide. In Figure 3c, we show the same synthetic contaminated with three different noise patterns.

In Figure 4a, we show the effect of applying a 3×3 running average mean filter to the image shown in Figure 3c. The overall signal-to-noise ratio is improved, but the fault edge is blurred and the fractures diminished.

The median and α-trimmed filters

The median filter is one of the most widely used nonlinear techniques in signal and image processing (Schulze and Pearce, 1991). In the seismic world, the median filter is routinely used in velocity filtering of VSP data to distinguish between downgoing and upgoing events using the differences in their apparent velocities. The median filter works by replacing each sample in a window of a seismic trace by the median of the samples falling within the analysis window. The window size is typically an odd number (e.g., 3×3 or 5×5). One way to calculate the median is simply to order all of the J samples in the analysis window using an ordering index k:

$$d_{j(1)} \leq d_{j(2)} \leq \cdots \leq d_{j(k)} \leq d_{j(k+1)} \cdots \leq d_{j(J)}. \quad (2)$$

The median is then given by

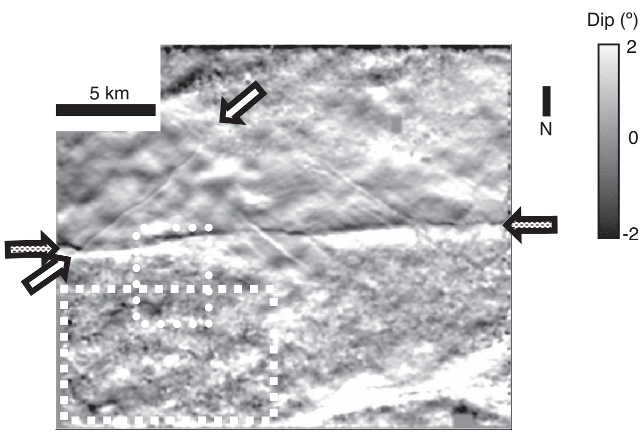

Figure 2. The result of applying four passes of 3×3 running-window mean filter on the data shown in Figure 1. Note that although a good deal of "random noise" has been rejected, the northwest-southeast lineaments and northeast-southwest channel are blurred.

$$d_{\text{median}} = d_{j[k=(J+1)/2]}. \quad (3)$$

The α-trimmed mean is given by:

$$d_\alpha = \frac{1}{(1-2\alpha)J} \sum_{k=\alpha J+1}^{(1-\alpha)J} d_{j(k)}, \quad (4)$$

where $0 \leq \alpha < 0.5$. If $\alpha = 0.5$, we replace equation 4 with the median filter. If $\alpha = 0.0$, we obtain the conventional mean filter.

The median filter is well known for preserving sharp discontinuities and removing impulse noise in the signal. The median and α-trimmed mean filters performs better than the mean filter in suppressing noise and preserving details, as seen by the improved fault edge shown in Figure 4b and c. However, neither of these two filters is capable of preserving the thin lineaments.

The edge-preserving smoothing (EPS) filter

Luo et al. (2002) applied Kuwahara et al.'s (1976) multiwindow filter to seismic data, resulting in an edge-preserving smoothing algorithm, which avoids smearing major discontinuities by using multiple overlapping windows. A statistic, such as the variance of the data, is evaluated in each of the overlapping windows. Then, the window with the best statistic (e.g., the minimum variance) is subjected to smoothing by using a mean, median, α-trimmed mean, or other filter. For widely spaced fault and channel edges, the chosen

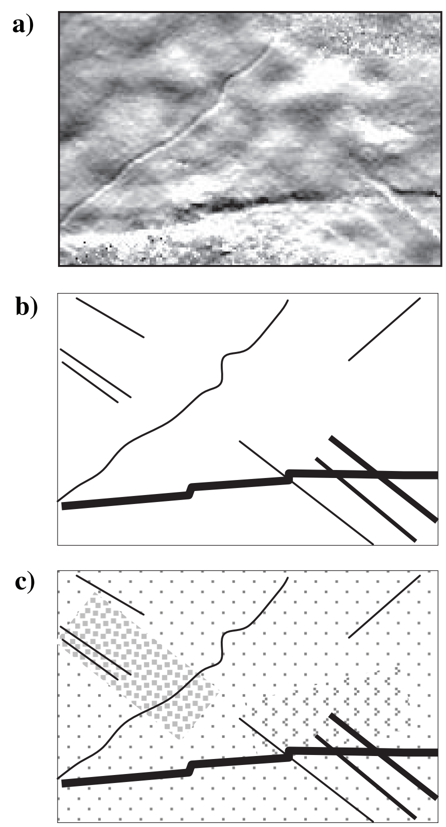

Figure 3. (a) A subsection of the northwest portion of the image shown in Figure 1. Idealized synthetics of the broad east-west strike-slip fault, northwest-southeast trending tension gashes, and a northeast-southwest trending meandering channel (b) without and (c) with additive noise.

window will not span a major discontinuity and therefore will not smooth across it. We show the effect of EPS using five overlapping 3×3 windows on the synthetic example shown in Figure 3c, applied to the window with the lowest variance (Figure 4d). Although the main fault is enhanced, the narrow lineaments are only partially illuminated.

The anisotropic diffusion filter

Hoeker and Fehmers' (2002) implementation of the anisotropic diffusion equation in their structure-oriented filter application is controlled by an estimate of the presence of discontinuities computed from the eigenvalues of a gradient structure tensor. Although we could use data-driven statistics based on the standard deviation, or alternatively, the range of the sample amplitudes that fall within each analysis window, as described by Perona and Malik (1990), we chose a much simpler interpreter-driven criterion of $\kappa = 1$ degree for the entire volume.

The filtered data is then given by the following formula:

$$d_{\text{filt}} = d_C + \frac{1}{2}\frac{1}{J-1}\sum_{j=1}^{J}(d_j - d_C)\exp\{-[(d_j - d_C)/\kappa]^2\}, \tag{5}$$

where d_C indicates the value at the center of the analysis window. Equation 5 shows that if κ is very large, we update the value of the center point by simply adding one-half the average difference between the value of the center point and the value of each of the other samples. For smaller values of κ, we weight our average to favor those values that are closer to the value of the center point. We apply equation 5 to the synthetic shown in Figure 3c, and obtain the result shown in Figure 4e. The lineaments are well preserved and the speckled noise is either rejected or smoothed.

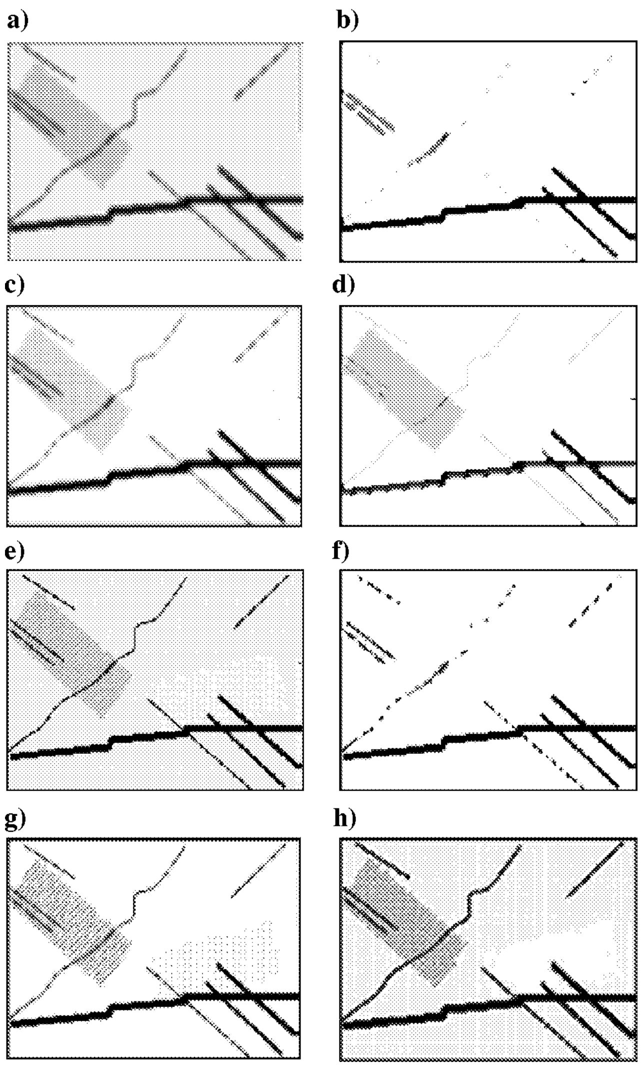

Figure 4. The image in Figure 3c after applying 3×3 running window filters: (a) mean, (b) median, (c) α-trimmed mean ($\alpha = 0.2$), (d) EPS (Kuwahara) (e) anisotropic diffusion, (f) LUM, (g) MSMTM with a moderate value of q, and (h) MSMTM with a small value of q. Note that although the mean, median, and α-trimmed filters preserve the wide east-west fault, the thinner lineaments are either unacceptably blurred or attenuated. In contrast, the anisotropic diffusion and MSMTM filters preserve these smaller features. The more aggressive LUM filter results in some holes in our lineaments.

The lower-upper-middle (LUM) filter

Boncelet et al. (1991) designed the LUM filter for smoothing and sharpening. Typically, they use a running 3×3 and 5×5 square window centered about each analysis point. The LUM filter calculates the median by the following two steps:

1) Sort the samples in the window as given by equation 2. As with the α-trimmed mean, the user defines lower and upper order statistics; only these values will be used in subsequent analysis. For our 3×3 window, we choose the lower and upper statistics to be the third and seventh ordered of the nine samples, or $k = 3$.
2) Compare the value of the center sample of the window d_C with these two order statistics. For smoothing, take the output to be the median of the lower order $d_{(k)}$, the upper order $d_{(N-k+1)}$ statistics and the center sample d_C:

$$d_{\text{LUM}}(k) = \text{med}(d_k, d_C, d_{N-k+1}). \tag{6}$$

Thus, the output will be d_C if the center value falls within the range of the "normal" values $[d_k, d_{N-k+1}]$. If this is not the case, the output will be the value of the two order-statistics d_k, d_{N-k+1} that is closer to d_C. Thus, "extreme" center values are brought in toward the normal values.

If $k = 1$, the output is always the same center value d_C. If $k = (N + 1)/2$, the output is always $d_{(N+1)/2}$, the median of the window. Therefore, the parameter k adjusts smoothing from none ($k = 1$), to that of a median $[k = (N + 1)/2]$. We illustrate this process through an example of 3×3 analysis in Figure 5.

Figure 4f shows the effect of LUM using a 3×3 window on the synthetic example in Figure 3c. Although the noise has been suppressed, the narrow lineaments, particularly the curvilinear channel, have been partially filtered out. They appear now to have holes in them.

The modified trimmed mean (MTM) filter

The modified trimmed-mean (MTM) filter — an enhancement of the α-trimmed mean filter — was designed by Lee and Kassam in 1985 to lessen the edge blurring typical of the standard mean filter. The modified trimmed-mean filter is also known as the range trimmed-mean filter. The MTM filter works sufficiently for some images; however, it cannot retain fine details of the image, such as point, lines, and curves. As a remedy, the MSMTM filter was developed and can be used equally as a noise filter.

Like the α-trimmed mean filter, the modified trimmed-mean filter is a running window estimator that selects only a subset of the samples inside the window to calculate an average. In this section, we simplify our notation by omitting the argument t (the indication of the time sample), with the understanding that the analysis window is either along a time or a horizon (interpreted reflector) slice including the analysis point. The samples d_j within the analysis window are selected if they fall within the following range:

$$d_{\text{median}} - q \le d_j \le d_{\text{median}} + q, \tag{7}$$

where d_{median} is given by equation 3, and q is a preselected threshold value between edge preservation and smoothing efficiency. Whereas the α-trimmed mean adds an equal number of ordered samples falling on either side of the median, the modified trimmed mean will, in general, add an unequal number of ordered samples on either side of the median, as defined by the value of the range q.

The result of the filter is the average of the selected samples:

$$d_{\text{MTM}} = \frac{1}{L}\sum_{j=1}^{J} b(d_{\text{median}}, q, d_j)d_j, \tag{8}$$

where $b(d_{\text{medain}}, q, d_j)$ is the boxcar function defined as

$$b(d_{\text{median}}, q, d_j) = \begin{cases} 1 & d_{\text{median}} - q \le d_j \le d_{\text{median}} + q \\ 0 & \text{otherwise,} \end{cases} \tag{9}$$

where L is the number of samples selected by the value q. If q has a value of zero, the resulting filter reduces to the median filter. As q increases, all of the samples of the window will eventually be included, such that the filter becomes the mean filter. Unfortunately, although the MTM filter is good for edge preservation, it is still based on the median and mean filters, and thus it cannot preserve internal details such as lineaments.

The multistage median (MSM) filter

The MSM filter was designed to enhance lineaments intersecting the center of the analysis window. By itself, it does a poor job of rejecting random noise on attribute images. However, we will use the MSM as the basis for a subsequent cascaded MSMTM filter discussed later. We calculate the multistage median d_{MSM} using the following four steps:

1) Define four 1D linear $(2N+1)\times 1$ subwindows W_p aligned in the north-south, east-west, northeast-southwest, and northwest-southeast of the larger 2D area $(2N+1)\times(2N+1)$ centered about the trace at (m,n):

$$W_1 = \{d(m+i,n), -N \le i \le N\},$$

$$W_2 = \{d(m+i,n+i), -N \le i \le N\},$$

$$W_3 = \{d(m,n+i), -N \le i \le N\},$$

and

$$W_4 = \{d(m+i,n-i), -N \le i \le N\}. \tag{10}$$

2) Calculate the median, $Z(W_p)$ of each of the four subwindows:

$$Z(W_p) = \text{median}[\mathrm{d}_{jk(\mathrm{W_p})}], \tag{11}$$

where the subscript $jk(W_p)$ denotes that sample d_{jk} falls within window W_p.

3) Calculate the second-stage medians defined as

$$M_{13} = \text{median}[Z(W_1), Z(W_3), d_{mn}],$$
$$M_{24} = \text{median}[Z(W_2), Z(W_4), d_{mn}], \tag{12}$$

where d_{mn} is the data value at the center of the analysis window.

4) Finally, calculate the final multistage median, d_{MSM}:

$$d_{\text{MSM}} = \text{median}[M_{13}, M_{24}, d_{mn}]. \tag{13}$$

The multistage median-based modified trimmed-mean (MSMTM) filter

Wu and Kundu (1991) combined the MTM filter with a detail-preserving filter, the multistage median filter, and dubbed the new filter the multistage median-based modified trimmed-mean (MSMTM). The MSMTM filter is an MTM filter based on a multistage median (MSM) filter. A data sample is selected if its value falls into the range of $[m-q, m+q]$, where m is a value calculated using the multistage median filter. Because the MSM filter is a detail-preserving filter, the MSMTM filter can preserve lineaments. The MSMTM filter is efficient, smooths noise, and preserves both edges and lineaments. Like all of the filters discussed in this paper, the MSMTM filter is implemented as a running window estimator. Like the α-trimmed mean and MTM filters, the MSMTM filter selects a subset of samples inside a window and calculates an average (Figure 6). Like the MTM algorithm, the samples are selected if they are in the range

$$d_{\text{MSM}} - q \le d_j \le d_{\text{MSM}} + q. \tag{14}$$

Note that we define our range with reference to the result of applying the multistage median (MSM) filter, d_{MSM}, rather than with reference to the median, d_{median}, as in equation 7.

The result of the filter is the average of the selected samples:

$$d_{\text{MSMTM}} = \frac{1}{L}\sum_{j=1}^{J} b(d_{\text{MSM}}, q, d_j)d_j. \tag{15}$$

We illustrate this process with an example of 3×3 analysis in Figure 6.

We show the effect of the MSMTM filter using a 3×3 window on the synthetic example shown in Figure 3c, using a moderate value of q in Figure 4g, and a small value of q in Figure 4h. For the moderate

-Sort the samples: $d_9, d_1, d_2, d_8, d_3, d_7, d_5, d_6, d_4$

$l = \{1\ 2\ 4\ 7\ 8\ 10\ 11\ 14\ 15\}$

-For parameters $k = 4$: $[d_{(k)}, d_{(N-k+1)}] = [\mathrm{d}_{(4)}, \mathrm{d}_{(6)}] = [7, 10]$

$d_{\text{LUM}}(k=4) = \text{median}(d_4, d_C, d_6) = \text{median}(7, 11, 10) = 10$

Figure 5. Example of the LUM filter; d_5 is the center sample.

value of q, there is some small smearing of the lineaments through the higher amplitude "noise" area. For the smaller value of q, the narrow lineaments are well preserved.

APPLICATION TO REAL DATA

In this section, we apply three of the more promising filters to a data set from the Fort Worth Basin that is faulted, fractured, and diagenetically altered. We find that, although the synthetic example shown in Figure 3c is helpful, the actual performance of these nonlinear filters is strongly dependent on the amplitude and spatial statistics of the noise to be suppressed as well as of the signal to be preserved. The faults and fractures (or lineaments) have little or no displacement or rotation about them. We speculate that their illumination by curvature attributes is related to velocity changes resulting from lateral changes in porosity, diagenetic alteration, gas charge, or crack cementation.

In our earlier work (Al-Dossary and Marfurt, 2006), we found that short-wavelength curvature estimates based on such dip volumes are particularly sensitive to short-wavelength noise. Therefore, we take our three best filters, anisotropic diffusion, LUM, and MSMTM, and apply them (four passes each) to the north-south and east-west component dip volumes. We display the north-south component of dip in Figure 7. Of the three filters, the MSMTM filter rejects high-energy salt and pepper noise but does not significantly alter the lineaments of interest.

Let us define a 3 x 3 window centered about the fifth sample d_5 :

$d_1 = 2$	$d_2 = 4$	$d_3 = 8$
$d_4 = 15$	$d_5 = 11$	$d_6 = 14$
$d_7 = 10$	$d_8 = 7$	$d_9 = 1$

After sorting the nine samples, we obtain the following:

d_9	d_1	d_2	d_8	d_3	d_7	d_5	d_6	d_4
1	2	4	7	8	10	11	14	15

Then :

$W_1 = \{d_2, d_5, d_8\} = \{4, 11, 7\}$ with $Z(W_1) = \text{median}(W_1) = 7$,

$W_2 = \{d_1, d_{5C}, d_9\} = \{2, 11, 1\}$ with $Z(W_2) = \text{median}(W_2) = 2$,

$W_3 = \{d_4, d_5, d_6\} = \{15, 11, 14\}$ with $Z_3 = \text{median}(W_3) = 14$,

$W_4 = \{d_3, d_5, d_7\} = \{8, 11, 10\}$ with $Z_4 = \text{median}(W_4) = 10$,

$M_{13} = \text{median}\ [Z(W_1), Z(W_3), d_C] = 11$,

$M_{24} = \text{median}\ [Z_{W2}, Z_{W4}, d_C] = 10$, and

$d_{MSM} = \text{median}\ [M_{13}, M_{24}, d_C] = 11$.

For $q = 3$, the selected samples are:

d_3	d_7	d_5	d_6
9	9	11	14

, such that

$d_{MSMTM} = \text{mean}\ (d_3, d_7, d_5, d_6) = 10.75$

Figure 6. Example of the MSMTM filter.

Curvature calculations are based on changes in dip and azimuth, and hence, exacerbate any noise present in the volumetric dip and azimuth estimates. Al-Dossary and Marfurt (2006) show that the short-wavelength estimates of curvature (using only nine–25 traces) are more sensitive to noise than the long-wavelength estimates (using between 100 and 400 traces). Therefore, we compute short-wavelength most-negative curvature using first derivatives of the original dip volume, as well as dip volumes that have undergone four passes of anisotropic diffusion, LUM, and MSMTM filtering. We display the results in Figure 8. The most-negative curvature image shown in Figure 8a is highly contaminated by random noise and acquisition footprint. Filtering the input data with anisotropic diffusion and

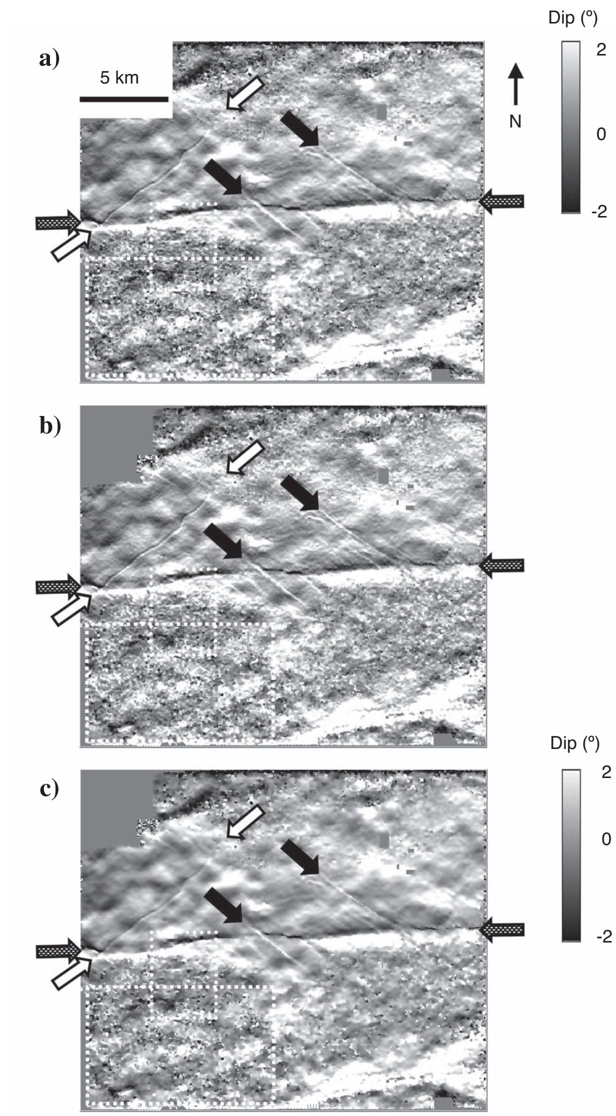

Figure 7. Filtered images of the data displayed in Figure 1 after four passes of a 3 × 3 window (a) anisotropic diffusion, (b) LUM, and (c) MSMTM filtering. Compare these to the image of the median-filtered data shown in Figure 2. Although the anisotropic diffusion and LUM filters behaved well on the synthetic images discussed in Figures 3 and 4, they did not reject a good deal of random noise. In contrast, the MSMTM image suppresses an amount of random noise similar to that seen in Figure 2, yet preserves the major lineaments without smearing them.

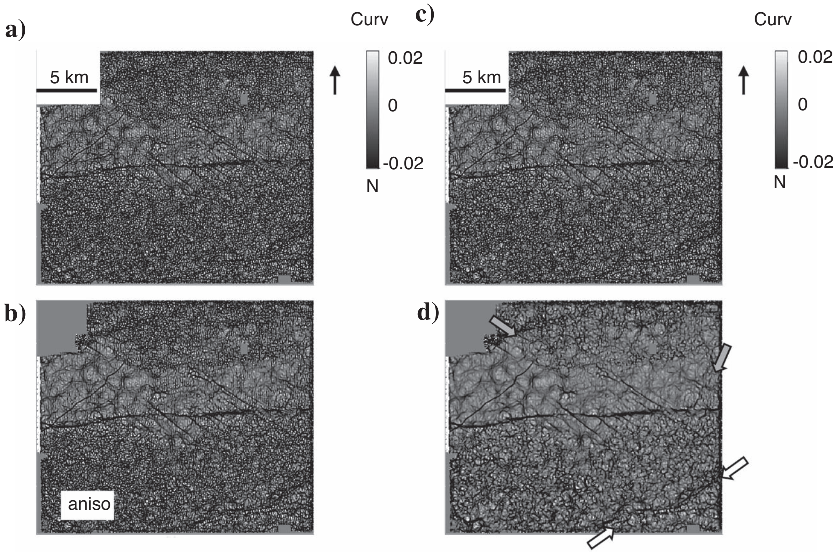

Figure 8. Time slices at $t = 0.8$ s through moderate wavelength ($\alpha = 0.75$) most negative curvature volumes calculated from volumetric estimates of dip and azimuth (a) without filtering (b) after four passes of anisotropic diffusion filtering, (c) after four passes of 3 $\times$ 3 window LUM filtering, and (d) after four passes of 3 $\times$ 3 window MSMTM filtering. The value of q for the MSMTM calculation was 1°, providing a moderate amount of smoothing. Note that the spectral content after MSMTM filtering is basically unchanged, and random noise and acquisition footprint are reduced, although lineaments of geologic interest are well preserved. White arrows indicate a fault associated with the Ouachita orogeny that can now be seen clearly. Gray arrows indicate subtle faults that were difficult to see in the original data.

LUM filters suppresses some of this noise (Figure 8b and c), but neither is as strong an improvement as the most negative curvature computed from the MSMTM-filtered data shown in Figure 8d. The north-south acquisition footprint is suppressed, as are many of the more random features, allowing us to see clearly the pattern of northwest-southeast and northeast-southwest faults and flexures.

CONCLUSIONS

Seismic attributes are sensitive to subtle changes in signal and noise, resulting in images that exacerbate the impact of backscattered noise and acquisition footprint. Popular random-noise-suppression algorithms, including mean, alpha-trim mean, and median filters, suppress random noise but may smear fault boundaries. Recently published structure-oriented filtering algorithms such as the multiwindow Kuwahara (or edge-preserving filtering) algorithm work well when the data are blocky, such as occurs between fault boundaries. Unfortunately, this algorithm blurs small linear features narrower than the analysis window that may be associated with joints and fractures. For this reason, we have evaluated a suite of noise-reduction algorithms used in image processing and SAR, including anisotropic diffusion, speckle-reducing, phase-preserving denoising, LUM, and MSMTM filters. Through testing (including the examples shown in this paper), we have found the multistage median-based modified trim-mean MSMTM filter to be superior in filtering volumetric dip estimates that form the basis of much of attribute analysis, including coherence, curvature, and lateral changes in reflectivity. The multistage median component of the MSMTM filter searches for and preserves constant value lineaments running through the analysis window. The range trimmed-mean component of the MSMTM filter improves signal-to-noise by smoothing data values that fall within a user-defined acceptable range. Because this algorithm requires sorting the sample values falling within each analysis window, the cost is about twice that of the simpler median filter, but much less than the cost of the original attribute computation. When applied to data from the Fort Worth Basin, Texas, we are able to identify faults and fractures on short-wavelength curvature images that are otherwise difficult to see.

Our experience shows that the MSMTM filter works well on attributes that have Gaussian statistics, such as dip, unnormalized amplitude gradients, and many of the curvature attributes. However, application of these filters to enhance lineations in attributes with non-Gaussian statistics, such as coherence, requires more research.

ACKNOWLEDGMENTS

The authors thank the sponsors of AGL and the Petroleum Research Fund for their support, and Devon Energy for permission to use their data. We also thank our geological colleagues at AGL, Peter Bartok, Chuck Blumentritt, and Charlotte Sullivan, for their enthusiasm, encouragement, and patience in explaining the use of curvature in structural interpretation. Saleh Al-Dossary wishes to thank Saudi Aramco for the opportunity and support in pursuing his graduate studies, especially Yi Luo, for his encouragement and support in pursuing this research.

REFERENCES

Al-Dossary, S., and K. J. Marfurt, 2006, 3D volumetric multispectral estimates of reflector curvature and rotation: Geophysics, **71**, no. 5, P41–P51.
Astola, J., and P. Kuosmanen, 1997, Fundamentals of nonlinear digital filtering: CRC Press.
Bahorich, M. S., and S. L. Farmer, 1995, 3D seismic discontinuity for faults and stratigraphic features: The coherence cube: The Leading Edge, **14**, 1053–1058.
Bakker, P., L. J. van Vliet, and P. W. Verbeek, 1999, Edge-preserving orientation adaptive filtering: Proceedings of the IEEE-CS Conference on Computer Vision and Pattern Recognition, 535–540.
Bergbauer, S., T. Mukerji, and P. Hennings, 2003, Improving curvature analyses of deformed horizons using scale-dependent filtering techniques: AAPG Bulletin, **87**, 1255–1272.
Blumentritt, C. H., K. J. Marfurt, and E. C. Sullivan, 2006, Volume-based curvature computations illuminate fracture orientations — Early to mid-Paleozoic, Central Basin Platform, west Texas: Geophysics, **71**, no. 5, B159–B166.
Boncelet, C., R. Hardie, and G. Arce, 1991, LUM filters for smoothing and sharpening, *in* E. R. Dougherty, G. R. Arce, and C. G. Boncelet Jr, eds, Nonlinear image processing II: Proceedings of SPIE, **1451**, 70–73.
Dalley, R. M., E. E. A. Gevers, G. M. Stampli, D. J. Davies, C. N. Gastaldi, P. R. Ruijetnberg, and G. J. D. Vermeer, 1989, Dip and azimuth displays for 3D seismic interpretation: First Break, **7**, 86–95.
Frost, V. S., J. A. Stiles, K. S. Shanmugan, and J. C. Hotzman, 1982, A model for radar images and its application to adaptive digital filtering of multiplicative noise: IEEE Transaction on Pattern Analysis and Machine Intelligence, **4**, 157–166.
Hoecker, C., and G. Fehmers, 2002, Fast structural interpretation with structure-oriented filtering: The Leading Edge, **21**, 238–243.
Kuwahara, M., K. Hachimura, S. Eiho, and M. Kinoshita, 1976, Digital processing of biomedical images: Plenum Press, 187–203.
Lee, J. S., 1986, Speckle suppression and analysis for synthetic aperture radar images: Optical Engineering, **25**, 636–643.
Lee, Y., and S. Kassam, 1985, Generalized median filtering and related nonlinear filtering techniques: IEEE Transactions on Acoustics, Speech, and

Signal Processing, **33**, 672–683.
Lisle, R. J., 1994, Detection of zones of abnormal strains in structures using Gaussian curvature analysis: AAPG Bulletin, **78**, 1811–1819.
Luo, Y., S. Al-Dossary, M. Marhoon, and M. Alfaraj, 2003, Generalized Hilbert transform and its application in geophysics: The Leading Edge, **22**, 198–202.
Luo, Y., W. G. Higgs, and W. S. Kowalik, 1996, Edge detection and stratigraphic analysis using 3D seismic data: 66th Annual International Meeting, SEG, Expanded Abstracts, 324–327.
Luo, Y., M. Marhoon, S. Al-Dossary, and M. Alfaraj, 2002, Edge-preserving smoothing and applications: The Leading Edge, **21**, 136–158.
Marfurt, K. J., 2006, Robust estimates of 3D reflector dip and azimuth: Geophysics, **71**, no. 4, P29–P40.
Perona, P., and J. Malik, 1990, Scale-space and edge detection using anisotropic diffusion: IEEE Transactions on Pattern Analysis and Machine Intelligence, **12**, 629–639.
Roberts, A., 2001, Curvature attributes and their application to 3D interpreted horizons: First Break, **19**, 85–99.
Schulze, M., and J. Pearce, 1991, Some properties of the two-dimensional pseudomedian filter, *in* E. R. Dougherty, G. R. Arce, and C. G. Boncelet Jr, eds, Nonlinear image processing II: Proceedings of SPIE, **1451**, 48–57.
Skirius, C., S. Nissen, N. Haskell, K. J. Marfurt, S. Hadley, D. Ternes, K. Michel, I. Reglar, D. D'Amico, F. Deliencourt, T. Romero, R. Romero, and B. Brown, 1999, 3D seismic attributes applied to carbonates: The Leading Edge, **18**, 384–389.
Sullivan, E. C., K. J. Marfurt, A. Lacazette, and M. Ammerman, 2006, Application of new seismic attributes to collapse chimneys in the Fort Worth Basin: Geophysics, **71**, no. 4, B111–B119.
Wu, W. R., and A. Kundu, 1991, A new type of modified trimmed mean filter, *in* E. R. Dougherty, G. R. Arce, and C. G. Boncelet Jr, eds, Nonlinear image processing II: Proceedings of SPIE, **1451**, 13–20.
Yu, Y., and S. Acton, 2002, Speckle reducing anisotropic diffusion: IEEE Transactions on Image Processing, **11**, 1260–1270.